Inorganic Chemistry Research

Article

Sonochemical Assisted Removal and Photocatalytic Degradation of Methylene Blue Dye by MIL-101(Cr) from Aqueous Solutions

Samaneh Hashemi Ghoochani[a], Abbas Heshmati[a], Hasan Ali Hosseini[a] and Majid Darroudi[b,c,*]

[a]*Chemistry Department, Payame Noor University, 19395-4697 Tehran, Iran*
[b]*Nuclear Medicine Research Center, Mashhad University of Medical Sciences, Mashhad, Iran*
[c]*Department of Medical Biotechnology and Nanotechnology, Faculty of Medicine, Mashhad University of Medical Sciences, Mashhad, Iran*

Received: May 27, 2021; Accepted: August 2, 2021
Cite This: *Inorg. Chem. Res.* **2021,** *5*, 230-237. DOI: 10.22036/icr.2021.288175.1105

Abstract: This study provides data on the performed synthesis of Metal-organic framework MIL-101(Cr) nanostructure through the application of a hydrothermal method. The prepared catalysts were characterized by the means of FESEM/ EDAX/PSA,FTIR , UV-Vis, BET, and XRD analyses. As the obtained XRD pattern approved the synthesis of MIL-101(Cr) by displaying diffraction peaks, the FESEM images also demonstrated the octahedral construction of this product. In addition, we evaluated the photocatalytic functionality and adsorption of MIL-101(Cr) for degrading methylene blue (MB) dye under UV light and dark conditions, respectively. According to the results, this product displayed an excellent potential for the removal of organic pollutants from aqueous solutions. However, the best outcomes were attained through the sonication method, since the structure and degradation properties of particles were improved due to the usage of chemical sonic.

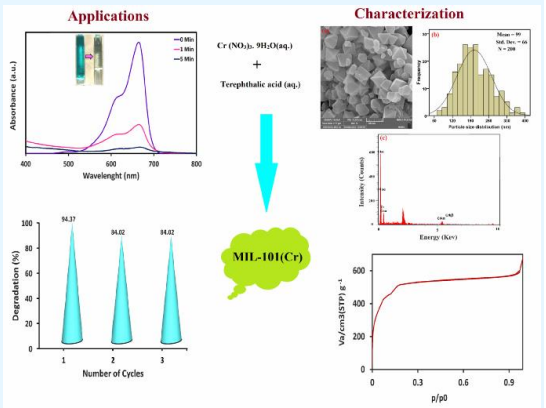

Keywords: Metal-organic framework MIL-101(Cr), Hydrothermal procedure, Photocatalytic activity, Water pollution, Sonication, Adsorption

1. INTRODUCTION

Throughout the recent years, water pollution remained a serious concern of the developing world and continues to stand as a threat by posing disastrous effects on the environment.[1,2] Several factors can cause water contamination including organic pollutants, pigmentation, and heavy metal ions.[3,4] The removal of these contaminations can occur through the usage of several materials including carbon nanotubes (CNTs), activated carbon, and MOFs.[5] Due to their fast rate of development, more than 20,000 MOFs were introduced in the past decade.[6] This material is consisted of two principal components as the following: a metal ion or cluster of metal ions and an organic molecule as a linker.[7] Considering their notable features, including high surface area, porosity, tenability, controllable pore size, crystalline structures, etc., the application of MOFs is applied in many different grounds such as adsorption, catalysis, drug delivery, and dye degradation.[8] Primarily, the active sorption sites of these products can be extended through their high surface areas (up to 3000 m^2 g^{-1}), high porosity (up to 1 cm^3 g^{-1}), and abundance of functional groups. Which can also facilitate photo-induced electron migration and ease the separation of charge carriers.[9] Furthermore, other linkers and metal ions can be added or switched with the organic linkers and metal nodes of MOFs, leading to the production of chemically and structurally diverse products. Dye adsorption is partially administered through the electrostatic interaction between the dye and adsorbent molecules since the mineralizing factor can cause a conversion in the charge that is elated by the framework of a dye solution.[9] MOFs can be exerted several times due to their uncomplicated separation from reaction systems,[10] which would result in spreading the lifetime of applied photocatalysts and decreasing the production of waste and pollution.[11] Known as an organic substance, a dye is consisted of two principal sections that include the presence of a chromophore, which stands accountable for manufacturing the color that increases its water

solubility.[12] Although this product is considered as a double-edged blade due to its vital functionality in certain industries such as leather, polymers, plastics refineries, and textiles leather,[13] yet their unleashed effluents are recognized as a hazardous threat to the health of humans and aquatic environment.[14] For instance, the exertion of MB dye is usually considered for coloring cotton, wool, and silk, however, the release of an even small amount of produced discharges into water bodies can cause negative consequences such as eye burning, vomiting, cyanosis.[14] Therefore, varying types of procedures were developed for dye removal, which includes advanced electrolysis, oxidation, catalytic reduction, membrane separation, catalytic reduction, photocatalytic degradation.[15] Among these methods, the processes of visible-light-driven photocatalyst and adsorption were proved to stand as the most applicable technologies in the field of cleaning and modifying the environment since they can provide high proficiency, low costs, and minimal damaging by-products, while requiring a low amount of energy.[16] In this research, MIL-101(Cr) was synthesized through the application of a hydrothermal procedure and characterized by the means of conventional methods including XRD, FESEM/EDAX/PSA, FTIR, UV-Vis, and BET. Next to investigating the photocatalyst activity and adsorption of MIL-101(Cr) on MB dye degradation, we also studied Sonochemical assisted removal as the novelty and innovation of our work. In the following, the kinetic of reactions was examined by evaluating the experimental results.

2. EXPERIMENTAL

Materials

In this experiment, we procured the required chromium(III) nitrate nonahydrate ($Cr(NO_3)_3.9H_2O$), N-N-dimethyl formamide (DMF), and methylene blue (MB) from Sigma-Aldrich company. Terephthalic acid and all of the utilized solvents were the products of Merck company.

Characterization

Various methods were applied to confirm the synthesis of MIL-101(Cr) nanostructure. The functional groups of MIL-101(Cr) were described by the application of FTIR analysis (Shimadzu-8400, Japan), while the optical studies of this nanostructure were investigated through UV-Visible spectrophotometry (HACH, DR 5000, USA). X-ray diffraction analysis was achieved by the means of XRD pattern (Philips Co. Holland), whereas FESEM/EDAX images (Hitachio S-4800) were employed to investigate the morphology and size of MIL-101(Cr). Furthermore, we evaluated the surface area of our product by performing the BET analyses (BELSORP Mini II).

Synthesis of MIL-101(Cr)

The successful synthesis of MIL-101(Cr) was achieved through the exertion of a hydrothermal method, in which the mixture of terephthalic acid (0.83 g, 5 mmol), $Cr(NO_3)_3.9H_2O$ (2.0 g, 5 mmol), and deionized water (20 mL) were sonicated while being ensued within a dark, blue-colored suspension. Thereafter, a Teflon-lined autoclave bomb was used to position the suspension in an oven at a temperature of 220 °C for 18 h without being stirred. Once the synthesis was completed, we separated the suspension by the application of a centrifuge (5,000 xg, 10 min). In order to remove the impurities, we sited the powder in DMF (20 mL) and had it sonicated for 10 min, which was retained afterward at 70 °C overnight. We separated the obtained product by executing numerous centrifugation processes, having the resultant washed with water, methanol, and acetone, and lastly allowing it to dry at 75 °C overnight.

Dye degradation

In this study, the mechanisms of adsorption, photocatalytic reaction, and sonication were selected and studies. For this purpose, different portions of MIL-101 (3, 15, and 30 mg in 100 mL) were added to MB solution (0.3 mg in 100 mL) in varying pH (6, 7, and 8) while being stirred (500 rpm). Meanwhile, the absorbance of solution was measured in different time intervals through a UV-Vis instrument. To investigate the experiments of photocatalytic dye degradation, a photoreactor was exerted along with a UV lamp (Philips 11w) with a wavelength of 365 nm to act as the source of irradiation. The experiments were completed by the application of varying ratios of MIL-101 as a nanocatalys while being stirred in 100 mL of MB solution at 25 °C. To examine the absorbance value of MB solution, the reaction was repeated at different time intervals. We measured the absorbance of solution by the usage of a UV-Vis instrument. All of the mentioned cases were also evaluated through the adsorption method in a dark place. To gather data on the sonication procedure, we sonicated the sample for 5 min and measured its absorbance value.

3. RESULTS AND DISCUSSION

X-ray diffraction (XRD)

Figure 1 displays the XRD patterns of synthesized MIL-101(Cr) by exerting a hydrothermal method and the XRD pattern of sample attained after the adsorption process, which was examined to determine the crystalline structure and sizes of this product.[16] The correspondence of this pattern with the reported XRD pattern ascertained the identity of synthesized substances to be MIL-101(Cr).[17] It should be noted that the XRD patterns of MIL-101(Cr) mostly demonstrated the distinctive peaks of MIL-101(Cr) at 2θ of 6.32, 11.14, 17.98°.[18] The existence of numerous pores throughout the construction of this porous material was denoted by observing intensive peaks at the small angles of XRD pattern. The value of crystallite size was measured by the application of Debye Scherrer equation (Eq. 1) to be 42.31 nm.[18]

$$D = \frac{k\lambda}{\beta \cos\theta} \qquad (1)$$

This equation controls the various characteristics of crystalline materials, in which D represents the crystal size, k = 0.9, λ refers to the wavelength of X-ray (0.154), θ would be the Braggs angle in radians, and β stands for the full width at half maximum of the peak in radians.[19]

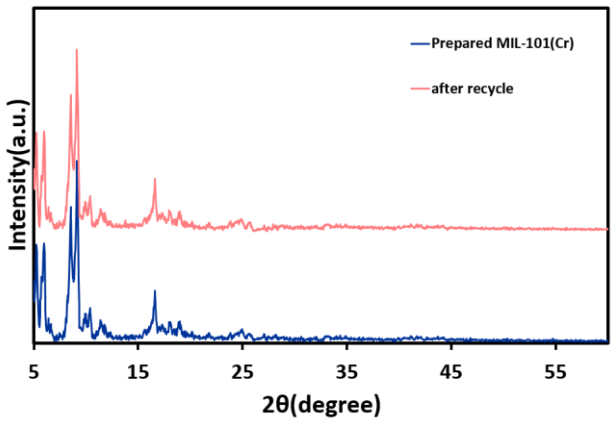

Figure 1. The XRD pattern of MIL-101(Cr).

Field emission electron microscopy (FESEM)

The application of FESEM/EDAX/PSA images was considered to study the shape, size, and elemental analysis of experimental sample.[20] In conformity to the FESEM/EDAX images of synthesized MIL-101(Cr), we observed the presence of crystals with spherical or semispherical and octahedral constructions (Figure 2a) with a mean diameter of about 203.8 nm (Figure 2b).[21] The prevalence of fine shapes and morphology of prepared MIL-101(Cr) proved the achievement of synthesized MOF. The appearance of Cr, C, O, and N elements in the structure of MOF was recorded in the EDAX spectrum of synthesized MIL-101(Cr) (Figure 2c).[22]

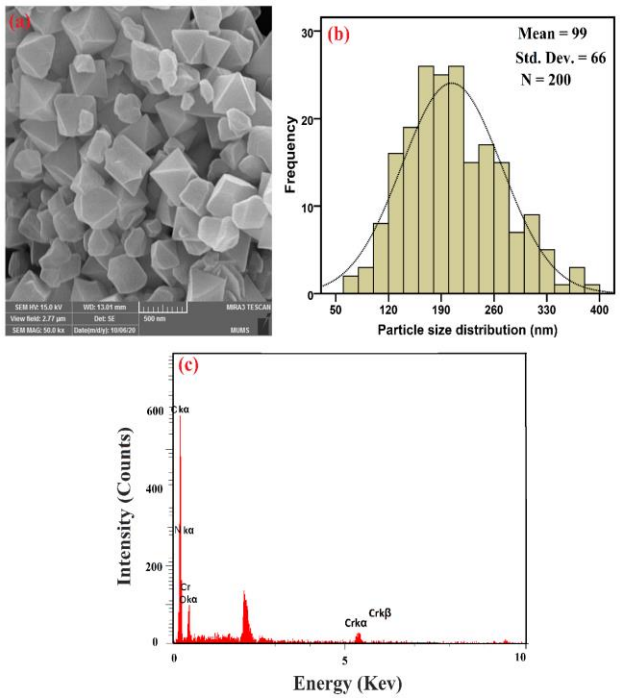

Figure 2. FESEM images (a), particle size distribution (b), and EDAX analyses of MIL-101(Cr) (c).

Fourier transforms infrared microscopy (FT-IR)

FT-IR analyses were used to point out the induced changes in functional groups that occurred during the synthesizing process.[23] According to the demonstrated results of MIL-101(Cr) FT-IR spectra in Figure 3, the displayed broadband at 3415 cm^{-1} is in agreement with the stretch vibrations of hydroxyl groups caused by the adsorbed water on the surface of particles. The detected band at 1398 cm^{-1} is similar to the symmetric (O–C–O) vibrations of dicarboxylate and the band at 1536 cm^{-1} is related to the asymmetric (C=O) stretching vibrations of dicarboxylate. These results confirmed the existence of a linker, benzene dicarboxylate, throughout the structure of MIL-101(Cr). The detected bands in the range of 600 to 1600 cm^{-1} belong to the benzene ring, which displayed the bending vibrations of C=C at 1255 cm^{-1}, the stretching vibrations of C=C at 1656 cm^{-1}, and the deformation vibrations of C–H at 1101, 1018, 883, and 748 cm^{-1}. Furthermore, the detected band at 2900 cm^{-1} was in correspondence with the bending vibrations of C–H, while the observed peak at 578 cm^{-1} was associated with the Cr–O vibrations.[24]

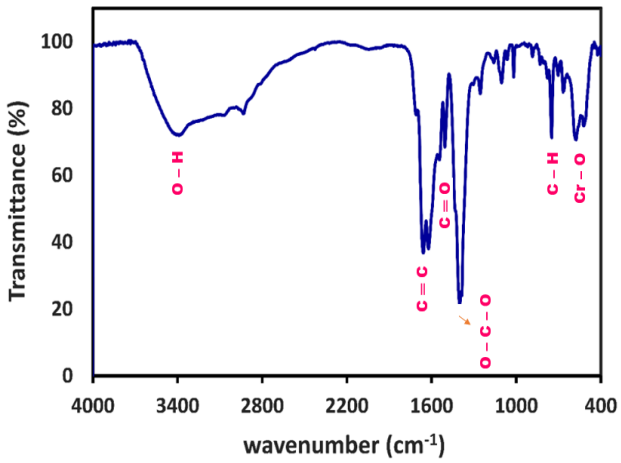

Figure 3. FTIR spectra of MIL-101(Cr).

UV-Vis and bandgap energy of MIL-101(Cr)

The UV-Vis diagram of synthesized MIL-101(Cr) exhibited a broad absorption band throughout the regions of 283 and 212 nm, which can be attributed to the d-d transition of Cr^{3+} ions (Figure 4a).[25] The bandgap energy of MIL-101(Cr) was obtained from the intercepts of the lines of $(\alpha h\upsilon)^2$ versus hν (Figure 4b). According to the Tauc equation (Eq. 2), the bandgap value of MIL-101(Cr) was calculated to be 3.55 eV.[26]

$$(\alpha h\nu)^n = A(h\nu - E_g) \qquad (2)$$

Where α signifies the absorption coefficient, h is the Planck's constant, υ would be the photon's frequency, A refers to a constant, E_g stands for the bandgap energy, and n represents an expression of a kind of optical transition.

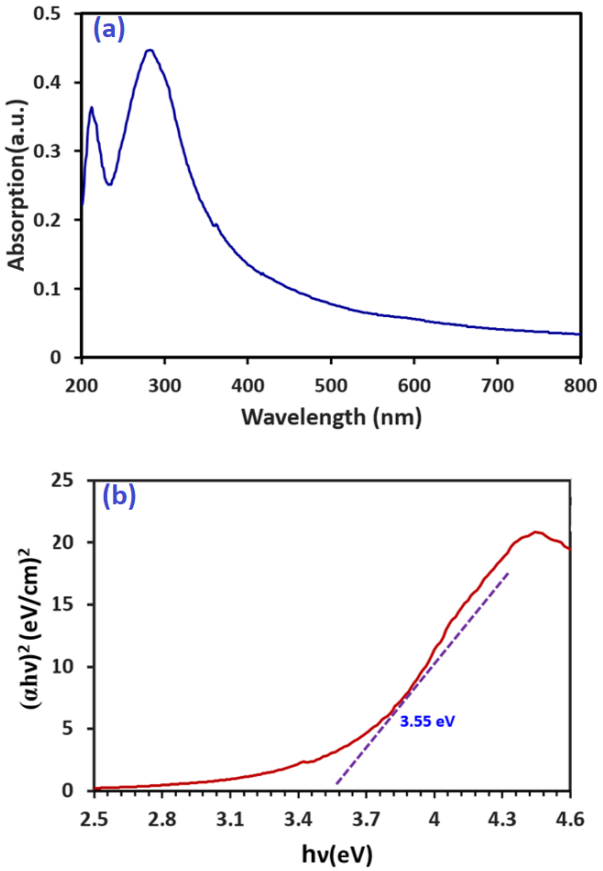

Figure 4. UV-Vis (a) Bandgap (b) spectra of MIL-101(Cr).

Brunauer-Emmett-Teller (BET) analysis

As it is provided in Figure 5, the application of BET analyses was considered to determine the surface area and pore diameter.[27] According to the adsorption-desorption of N_2, the surface area of MIL-101 was recorded to be 2282.9 m^2 g^{-1}, while the pore size was about 2.52 nm.[28] In addition, the total pore volume was obtained to be 1.44 cm^3 g^{-1} and demonstrated in (Table 1).

Table 1. Surface area, pore size, and total pore volume of the MIL-101(Cr)

Sample	Surface area (m^2 g^{-1})	Pore size (nm)	Total pore volume (p/p_0 = 0.990)
MIL-101	2282.9	2.52	1.44

Effective parameters on dye degradation

There is a large number of varying parameters that can affect the progress of dye degradation, which includes catalyst dosage, initial dye concentration, and pH in various conditions.[29]

The photocatalytic activity

The rate of decolorization was observed to face an increase over time under UV light, which is almost

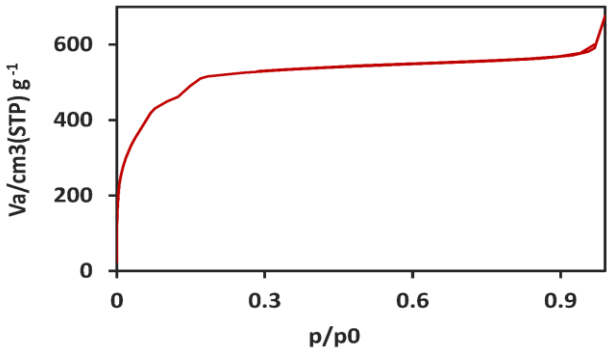

Figure 5. BET analyses of MIL-101(Cr).

identical to the bleaching outcomes that were achieved by the application of UV light (Table 2). The gathered results were indicative of 91.10% of decolonization, which was attained through the exertion of UV (Figure 7). The photocatalysis mechanism of synthesized MIL-101(Cr) is presented in Figure 6.[17] In a case where the UV light energy is greater than or equal to the nanoparticle bandgap energy, the electron transitions of valence band are excited towards the conduct band and lead to the creation of a hole (h^+) in the valence band and an electron (e^-) in the conduct band. The holes on the valence band react with water molecules (H_2O) or hydroxyl ions (OH^-) and form hydroxyl radicals (OH°), while the oxygen molecules (O_2) react with the electron of conduct band (e^-) to produce superoxide radical anions ($O_2^{-\circ}$). These superoxide radical anions ($O_2^{-\circ}$) and hydroxyl radicals (OH°) are active species that can react with MB dye and initiate the process of dye degradation. Thus, the photochemical degradation mechanism is consisted of the following reaction 1 to 6:

$$MIL-101(Cr) + h\nu \rightarrow MIL-101(Cr)^* + e^{\pm h+} \quad (1)$$

$$h^+ + H_2O \rightarrow H^+ + OH^\circ \quad (2)$$

$$h^+ + OH^- \rightarrow OH^\circ \quad (3)$$

$$e^- + O_2 \rightarrow O_2^- \quad (4)$$

$$OH^{-\circ} + MB \rightarrow Degradation products \quad (5)$$

$$O_2^{-\circ} + MB \rightarrow Degradation products \quad (6)$$

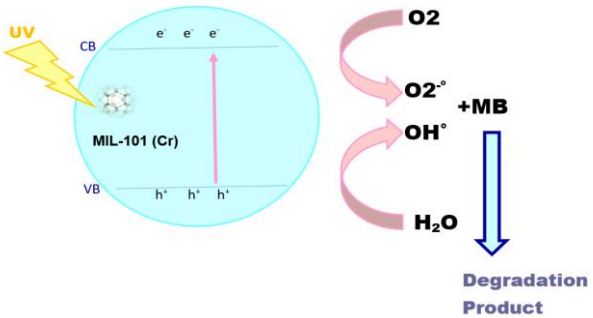

Figure 6. Schematic plan of MIL-101(Cr) photocatalytic mechanism.

Table 2. The photocatalytic activity of MIL-101(Cr); Condition: UV, catalyst dosage = 300 ppm and pH = 7

Catalyst	Time (min)	Absorbance	Yield (%)
MIL-101(Cr)	0	0.551	-
MIL-101(Cr)	1	0.317	42.46
MIL-101(Cr)	3	0.158	71.32
MIL-101(Cr)	5	0.11	80.03
MIL-101(Cr)	10	0.094	82.94
MIL-101(Cr)	20	0.081	85.29
MIL-101(Cr)	30	0.069	87.47
MIL-101(Cr)	45	0.054	90.19
MIL-101(Cr)	60	0.049	91.10

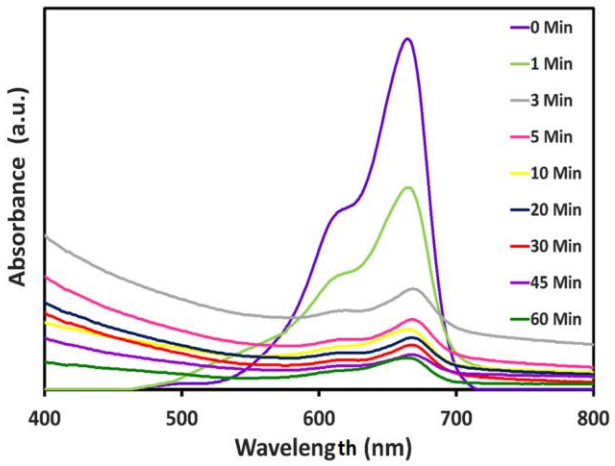

Figure 7. The UV-Vis spectral changes of MB during photocatalytic dye degradation at different reaction times for MIL-101(Cr).

Adsorption of MB

The obtained yield of dye degradation by the usage of MIL-101(Cr) and lack of UV irradiation was 90.92% after 60 min (Figure 8). The adsorption of MB dye in MIL-101(Cr) (42.46%) during the first minute was rapid, which was predictable due to its high surface areas (Table 3). To be described in detail, MB molecules have the potency to efficiently pass over the border layer and easily diffuse the external layer of adsorbent to rapidly end up trapped within the pores of MIL-101(Cr). In conformity to the gathered data, the cavities were filled with MB since its adsorption decreases as the contact time increases, the adsorption data of MIL-101(Cr) was fairly similar to these results except for the amount of adsorption, which was reported to be 90.92 % (Table 3).

Table 3. Adsorption of MIL-101(Cr) catalyst

Condition	Catalyst dosage (ppm)	pH	Time (min)	Absorbance	Yield (%)
Adsorption	300	7	0	0.551	-
Adsorption	300	7	1	0.317	42.46
Adsorption	300	7	3	0.199	63.88
Adsorption	300	7	5	0.186	66.24
Adsorption	300	7	10	0.119	78.40
Adsorption	300	7	20	0.1	81.85
Adsorption	300	7	30	0.083	84.93
Adsorption	300	7	45	0.067	87.84
Adsorption	300	7	60	0.05	90.92

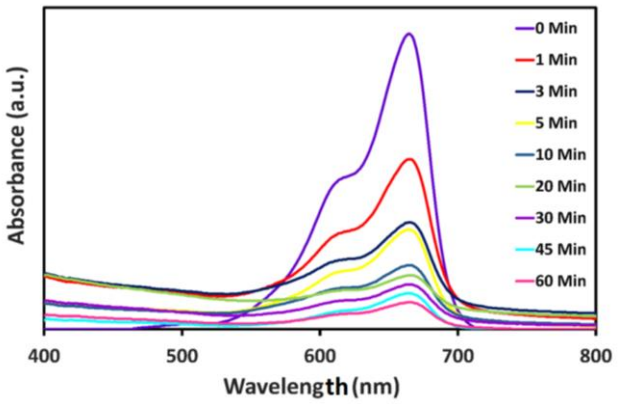

Figure 8. The UV-Vis spectral changes of MB during dye adsorption at different reaction times for MIL-101(Cr).

The value of yield after 5-min of sonication was 94.37%, which is considered to be the best result since the removal of MB dye decreases in the first five minutes as it is displayed in Table 4; however, the occurrence of desorption over time is inevitable. Therefore, when being compared to the required 60 min in other methods, the significant result of sonication method was achieved in 5 min. In conformity to these outcomes, sonication can yield a notable percentage of dye degradation when being compared to the results of UV and dark procedures (Figure 9).

Table 4. The effect of MIL-101(Cr) sonication

Condition	Catalyst dosage (ppm)	pH	Time (min)	Absorbance	Yield (%)
Sonication	300	7	0	0.551	-
Sonication	300	7	1	0.143	74.04
Sonication	300	7	5	0.031	94.37

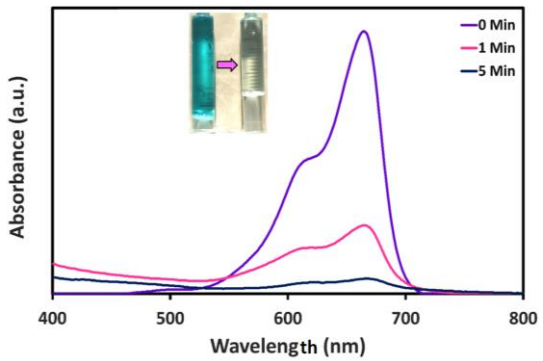

Figure 9. The effect of sonication on UV-Vis spectral changes of MB removal.

The effect of pH

The related experiments were executed at the varying conditions of acidic, basic, and natural pH values (6,7,8). Initially, the degradation was observed to be more effective as the pH was increased. However, the optimum result of this paper was obtained in 5 min at the pH = 7 although due to the cationic nature of MB, it was sensible

to observe better results at the pH = 8.[30] Considering how the surface of nanoparticles is commonly positively charged, it is comprehensible to achieve a lower adsorption of MB at pH = 6. As it is displayed in Figure 10**,** the best result was achieved at the PH = 7 and reported to be 94.37%, which is higher than the outcomes of pH = 6 (41.01%) and pH = 8 (94.19%).

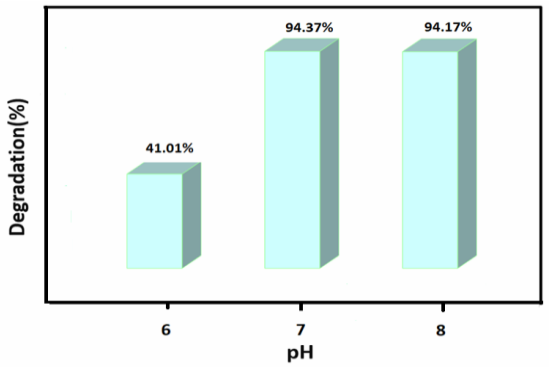

Figure 10. Effects of pH on the degradation of MB at 5 min and 300 ppm.

The effect of concentration

The experiment was performed with different concentrations and according to Figure 11, the best results were related to the concentration of 300 ppm (94.37%). We observed the inducement of less discoloration at a concentration of 150 ppm (87.29%), while the degradation percentage was reported to be 71.14% at 30 ppm.

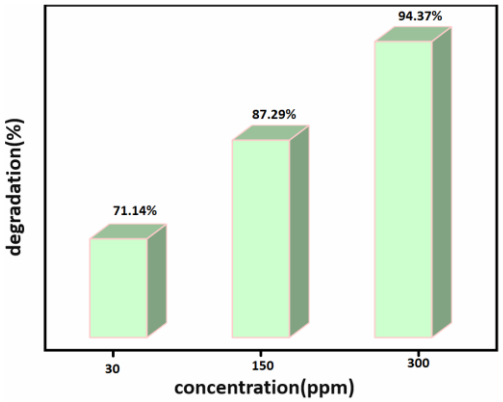

Figure 11. Effects of concentration on the degradation of MB at pH = 7.

Dye degradation kinetics

Pseudo-second-order kinetic models were exerted to investigate the kinetics of adsorption and photodegradation of MB dye, which required the usage of following Eq. 3.[31]

$$([MB])^{-1} = k_2 t + ([MB])_0^{-1} \qquad (3)$$

Where [MB] and $[MB]_0$ characterize the concentration of MB at time zero and time t. The adsorption of MB by MIL-101(Cr) was compatible with the rate of pseudo-second-order reaction, in which the rate constant was achieved to be 0.2846 M^{-1} min^{-1} (Figure 12a).[17] Also, the rates of photodegradation reaction for MIL-101(Cr) were detected to involve pseudo-second-order photocatalytic kinetics, which resulted in the rate constant of 32.092 M^{-1} min^{-1} (Figure 12b).

Degradation comparison

As the last section, the obtained results of dye degradation from the present catalyst were compared with some other literature of removing contaminations (Table 5). Accordingly, MIL-101(Cr) displays a high degradation percentage within the least required time interval.

MIL-101 reusability and stability

In regard to the recycling of MIL-101(Cr), we exerted distilled water for four rounds and utilized the prepared catalyst again for three turns (94.39, 84.02, 84.02, and 80.58%) throughout the sonication method. According to the outcomes, the catalytic activity of MIL-101(Cr) was decreased by about 10 % in the first round, remained stable for the second time, and slightly decreased in the following turn. The testing results of MIL-101(Cr) reusability are presented in (Figure 13). The results of stability testing in ambient conditions over a number of days are provided in (Figure 14). Generally, the main distinctive peak of MIL-101(Cr) can be detected throughout the UV spectrum.[35]

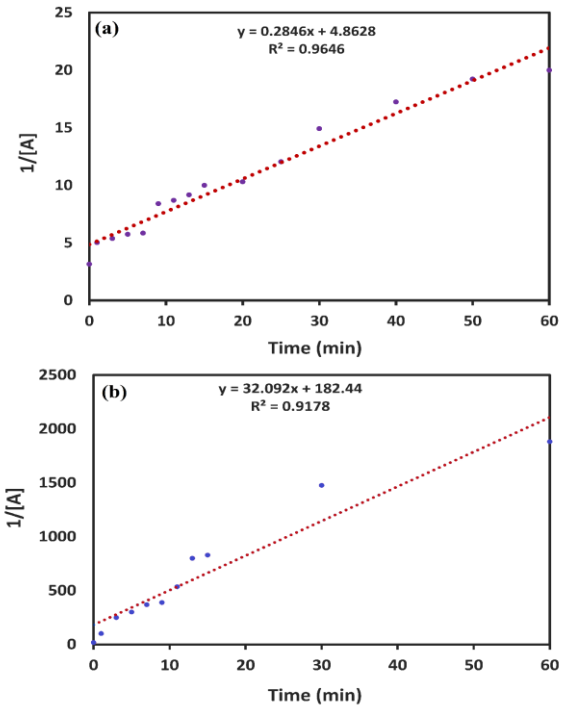

Figure 12. diagram of pseudo-second-order adsorption kinetics of MIL-101 (a) diagram of pseudo-second-order photocatalytic kinetics of MIL-101 (b).

Table 5. Comparison of the degradation of current MIL-101(Cr) and the available result

Catalyst	Condition	Contamination	Time (min)	Degradation (%)	Ref.
MIL-101(Cr)	UV	MB	60	91.10	This work
MIL-101(Cr)	Dark	MB	60	90.92	This work
MIL-101(Cr)	Sonication	MB	5	**94.37**	This work
ED-MIL-101(Cr)	Dark	Pb(II)	30	97.22	32
MIL-101(Cr)-NH_2-Co(II) PC	Dark	Alcohol	480	91	33
MIL-101(Cr)	Dark	*RBB	15	43	17
MIL-101(Cr)	UV	RBB	45	100	17
TiO_2/Salicylaldehyde-NH_2-MIL-101(Cr)	UV	Atenolol	60	75	34
TiO_2/Salicylaldehyde-NH_2-MIL-101(Cr)	Visible light	Atenolol	60	82	34

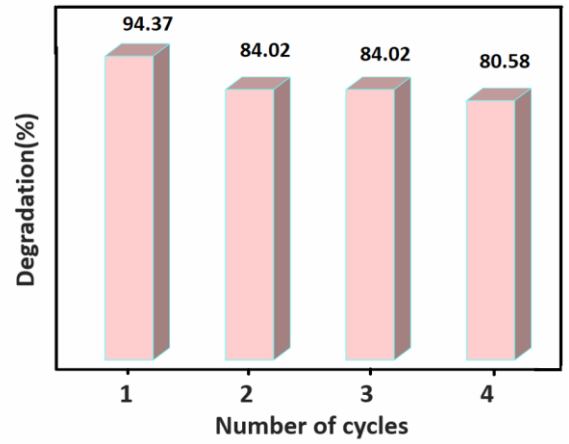

Figure 13. MB degradation efficiencies of recycled catalysts.

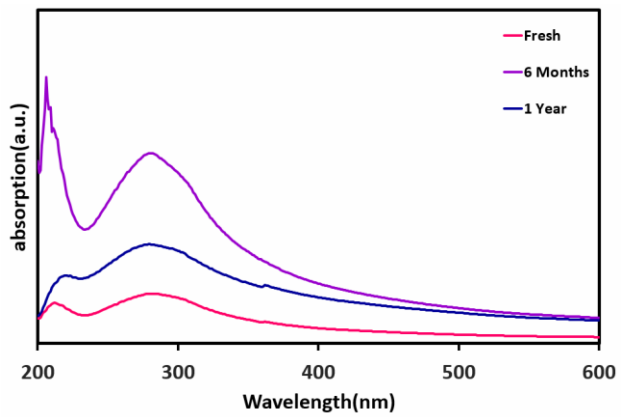

Figure 14. Stability experiment of MIL-101 in ambient conditions over different days.

4. CONCLUSIONS

This work reports the synthesis of MIL-101(Cr) that was achieved by performing a hydrothermal procedure. We also provide data on the usage of this product as a catalyst for photocatalytic degradation, adsorption, and discussed the effect of sonication in regards to MB dye. The decolorization results were directly associated with the exerted catalyst or dosage of adsorbent. In addition, although an increase in the pH of wastewater caused a positive influence on dye decolorization, yet the optimum conditions were affirmed to require continuous stirring for 5 min at the pH = 7 in room temperature through the performance of a sonication method. Recycling the catalyst and adsorbent was observed to cause insignificant changes in the efficiency of sonication processes. Confirmed by the gathered outcomes, the prepared MIL-101(Cr) can be recycled and act as an effective adsorbent at a neutral pH. In addition, its efficacy in MB removal can be applicable in industrial applications by offering economic benefits for the future of wastewater treatments. Nevertheless, this discovery needs to be thoroughly evaluated and further assessed to be appropriately improved in future studies.

CONFLICTS OF INTEREST

The authors declare no competing interests.

AUTHOR INFORMATION

Corresponding Author

Majid Darroudi: Email: darroudim@mums.ac.ir, majiddarroudi@gmail.com, ***ORCID***: 0000-0002-2624-7242

Author(s)

Samaneh Hashemi Ghoochani, Abbas Heshmati, Hasan Ali Hosseini

ACKNOWLEDGEMENTS

The technical support for this work was provided by Payame Noor University of Mashhad and Mashhad University of Medical Sciences based on the Ph.D. thesis of Ms. Samaneh Hashemi Ghoochani.

REFERENCES

1. A. Inyinbor Adejumoke, O. Adebesin Babatunde, P. Oluyori Abimbola, A. Adelani Akande Tabitha, O. Dada Adewumi, A. Oreofe Toyin, Water Challenges of an Urbanizing World, **2018**, 33-53.
2. Z. Sabouri, A. Akbari, H. A. Hosseini, M. Khatami, M. Darroudi, *Green Chem. Lett. Rev.* **2021**, *14*, 404-414.
3. J. Briffa, E. Sinagra, R. Blundell, *Heliyon*, **2020**, *6*, e04691.
4. Z. Sabouri, M. Sabouri, M. S. Amiri, M. Khatami, M. Darroudi, *Mater. Technol.* **2020**, 1-14.
5. S. Dhaka, R. Kumar, A. Deep, M. B. Kurade, S. -W. Ji, B. -H. Jeon, *Coord. Chem. Rev.* **2019**, *380*, 330-352.
6. W. -H. Li, W. -H. Deng, G. -E. Wang, G. Xu, *Energy Chem.* **2020**, *2*, 100029.
7. A. E. Thorarinsdottir, T. D. Harris, *Chem. Rev.* **2020**, *120*, 8716-8789.

8. W. Cai, C. C. Chu, G. Liu, Y. X. J. Wáng, *Small.* **2015**, *11*, 4806-4822.
9. B. Li, H. M. Wen, Y. Cui, W. Zhou, G. Qian, B. Chen, *Adv. Mater.* **2016**, *28*, 8819-8860.
10. J. Jiao, W. Gong, X. Wu, S. Yang, Y. Cui, *Coord. Chem. Rev.* **2019**, *385*, 174-190.
11. H. Zangeneh, A. Zinatizadeh, M. Habibi, M. Akia, M. H. Isa, *J. Ind. Eng. Chem.* **2015**, *26*, 1-36.
12. H. S. Rai, M. S. Bhattacharyya, J. Singh, T. Bansal, P. Vats, U. Banerjee, *Crit. Rev. Environ. Sci. Technol.* **2005**, *35*, 219-238.
13. A. S. Eltaweil, E. M. Abd El-Monaem, G. M. El-Subruiti, M. M. Abd El-Latif, A. M. Omer, *RSC Adv.* **2020**, *10*, 19008-19019.
14. K. Meerbergen, K. A. Willems, R. Dewil, J. Van Impe, L. Appels, B. Lievens, *J. Biosci. Bioeng.* **2018**, *125*, 448-456.
15. K. Piaskowski, R. Świderska-Dąbrowska, P. K. Zarzycki, *J. AOAC Int.* **2018**, *101*, 1371-1384.
16. S. M. Mirsoleimani-azizi, P. Setoodeh, F. Samimi, J. Shadmehr, N. Hamedi, M. R. Rahimpour, *J. Environ. Chem. Eng.* **2018**, *6*, 4653-4664.
17. P. D. Du, H. T. M. Thanh, T. C. To, H. S. Thang, M. X. Tinh, T. N. Tuyen, T. T. Hoa, D. Q. Khieu, *J. Nanomate*r. **2019**, *2019*.
18. U. Holzwarth, N. Gibson, *Nat. Nanotechnol.* **2011**, *6*, 534-534.
19. R. Kroon, S. *Afr. J. Sci.* **2013**, *109*, 01-02.
20. A. Samadi-Maybodi, M. Nikou, *Polyhedron.* **2020**, *179*, 114342.
21. H. A. Isiyaka, K. Jumbri, N. S. Sambudi, Z. U. Zango, B. Saad, A. Mustapha, R. *Soc. Open Sci.* **2021**, *8*, 201553.
22. L. Nirumand, S. Farhadi, A. Zabardasti, A. Khataee, *Ultrason. Sonochem.* **2018**, *42*, 647-658.
23. M. Shafiei, M. S. Alivand, A. Rashidi, A. Samimi, D. Mohebbi-Kalhori, *Chem. Eng. J.* **2018**, *341*, 164-174.
24. S. Kayal, A. Chakraborty, *Chem. Eng. J.* **2018**, *334*, 780-788.
25. F. Chen, W. An, Y. Li, Y. Liang, W. Cui, *Appl. Surf. Sci.* **2018**, *427*, 123-132.
26. Y. Tang, X. Yin, M. Mu, Y. Jiang, X. Li, H. Zhang, T. Ouyang, *Beilstein Arch.* **2019**, *2019*, 141.
27. X. Zhou, W. Huang, J. Shi, Z. Zhao, Q. Xia, Y. Li, H. Wang, Z. Li, *J. Mater. Chem. A* **2014**, *2*, 4722-4730.
28. Q. Liu, L. Ning, S. Zheng, M. Tao, Y. Shi, Y. He, *Sci. Rep.* **2013**, *3*, 1-6.
29. V. K. Gupta, R. Jain, A. Mittal, T. A. Saleh, A. Nayak, S. Agarwal, S. Sikarwar, *Mater. Sci. Eng.: C*, **2012**, *32*, 12-17.
30. E. S. Dragan, D. F. Apopei, *Chem. Eng. J.* **2011**, *178*, 252-263.
31. S. Senthilkumaar, P. Varadarajan, K. Porkodi, C. Subbhuraam, *J. Colloid Interface Sci.* **2005**, *284*, 78-82.
32. X. Luo, L. Ding, J. Luo, *J. Chem. Eng. Data.* **2015**, *60*, 1732-1743.
33. A. Shaabani, R. Mohammadian, A. Hashemzadeh, R. Afshari, M. M. Amini, *New J. Chem.* **2018**, *42*, 4167-4174.
34. Z. Mehrabadi, H. Faghihian, *J. Photochem. Photobiol.: A* **2018**, *356*, 102-111.
35. Z. Sabouri, A. Rangrazi, M. S. Amiri, M. Khatami, M. Darroudi, *Bioprocess Biosyst. Eng.* **2021**, https://doi.org/10.1007/s00449-021-02613-8.